Comparative Density-Functional Study of the Electron Paramagnetic Resonance Parameters of Amavadin

Christian Remenyi,[†] Markéta L. Munzarová,[‡] and Martin Kaupp*[,†]

Institut für Anorganische Chemie, Universität Würzburg, Am Hubland, D-97074 Würzburg, Germany, and National Centre for Biomolecular Research, Faculty of Science, Masaryk University, Kotlářská 2, CZ-61137 Brno, Czech Republic

Received: October 25, 2004; In Final Form: December 3, 2004

Electronic **g** tensors and hyperfine coupling tensors have been calculated for amavadin, an unusual eight-coordinate vanadium(IV) complex isolated from *Amanita muscaria* mushrooms. Different density-functional methods have been compared, ranging from local via gradient-corrected to hybrid functionals with a variable Hartree−Fock exchange admixture. For both electron paramagnetic resonance (EPR) properties, hybrid functionals with an appreciable exact-exchange admixture provide the closest agreement with experimental data. Second-order spin−orbit corrections provide non-negligible contributions to the ^{51}V hyperfine tensor. The orientation of **g** and **A** tensors relative to each other also depends on spin−orbit corrections to the **A** tensor. A rationalization for the close resemblance of the EPR parameters of amavadin to those of the structurally rather different vanadyl complexes is provided, based on the nature of the relevant frontier orbitals.

1. Introduction

Amavadin is a vanadium(IV) complex with an unusual structure and metal−ligand bonding mode (cf. Figure 1). It was first extracted in 1972 from *Amanita muscaria* type mushrooms.[1] Its pronounced accumulation is responsible for the distinct vanadium EPR spectra found with any part of these mushrooms. The biological role of amavadin is still unclear. The EPR and UV/vis spectra of either the mushrooms themselves or the complex isolated from them are closely similar to those of the well-known vanadyl(IV)-type complexes, in which a vanadium−oxo moiety is present.[2−4] This is the main reason amavadin was, for many years, thought to be a vanadyl complex. Only the structural characterization of related model complexes and eventually of amavadin itself showed that the structure is rather different (Figure 1): four carboxylate donor positions and two η^2-bonded hydroxylamino groups of the hidpa ligand [hidpa = trifold deprotonated trianion of 2,2′-(hydroxyimino)diacetic acid] lead to an unusual eight-coordinate complex.[5−9] Progress in the investigation of amavadin was reviewed by Garner et al.[10]

Based on DV Xα studies, it has been suggested that the close similarity of the amavadin optical spectra to those of vanadyl-(IV) complexes is due to a similar magnitude of the electronic influence of the two η^2 N−OH ligands in the former compared to one oxo ligand in the latter.[11] Does this also hold for the similarity in the EPR spectra? Recent systematic studies of both **g** tensors and hyperfine tensors of transition-metal complexes have shown that density-functional theory (DFT) provides a useful basis for the calculation of both properties.[12−21] However, a rather pronounced dependence of the results on the exchange-correlation functional was found. For example, gradient-corrected or local functionals underestimate core−shell spin polarization at the metal, which is important in the calculation of isotropic-metal hyperfine coupling constants (HFCCs).

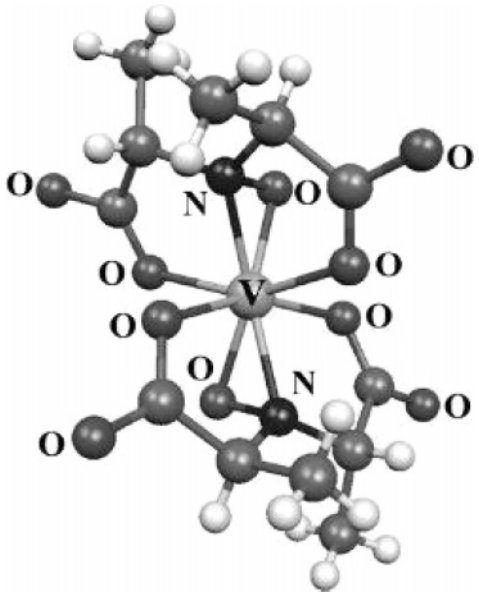

Figure 1. Structure of amavadin, $[V(hidpa)_2]^{2-}$ (cf. ref 5).

Similarly, deviations of the **g** tensor from the free-electron value are also significantly underestimated by generalized-gradient-approximation (GGA) or local-density-approximation (LDA) functionals in typical paramagnetic transition-metal complexes with metal-centered spin density (cf. ref 19 for more exceptional cases). Hybrid functionals may improve the core−shell spin polarization and, thus, often give better metal hyperfine couplings.[20] They may also provide improved agreement with experimental values for **g** tensor components.[19,21] However, in neither case was the improvement without exceptions. In particular, an increased admixture of Hartree−Fock (HF) exchange may be coupled to spin contamination in unrestricted treatments, which, under certain circumstances, deteriorates computed hyperfine tensors and **g** tensors [when the singly occupied molecular orbitals (SOMOs) are significantly metal−

* Corresponding author. E-mail: kaupp@mail.uni-wuerzburg.de.
[†] Universität Würzburg.
[‡] Masaryk University.

10.1021/jp045148+ CCC: $30.25
Published on Web 02/08/2005

ligand antibonding].[20] Note that a recently reported, more appropriate "localized" self-consistent implementation of hybrid functionals within the optimized-effective-potential framework[22−25] does not eliminate the spin-contamination problem per se but removes the associated deterioration of **g**-tensor data for 3d complexes.[25]

Here, we take amavadin as an interesting test case (a) to judge the performance of different DFT methods for both hyperfine coupling and **g** tensors, (b) to estimate the importance of spin−orbit (SO) coupling effects, even for the HFCC of a relatively light metal like vanadium, (c) to analyze, in detail, the orientation of the two tensors, and (d) to better understand the similarity of the amavadin EPR parameters to those of vanadyl complexes (DFT studies of EPR parameters of vanadyl(IV)[26,27] and vanadocene(IV)[28] systems have been carried out previously).

2. Theoretical Formalism and Computational Details

Formalism of g-Tensor Calculations. The theoretical background of EPR parameters is covered in detail in textbooks.[29−34] Hence, we summarize only the most relevant points. The **g** tensor is calculated as a correction to the free-electron value (given in ppt, i.e., in units of 10^{-3}):

$$\mathbf{g} = g_e\mathbf{1} + \Delta\mathbf{g} \tag{1}$$

with $g_e = 2.002\,319$. Up to the level of second-order perturbation theory based on the Breit−Pauli Hamiltonian, the **g**-shift $\Delta\mathbf{g}$ consists of three terms:

$$\Delta\mathbf{g} = \Delta\mathbf{g}^{SO/OZ} + \Delta\mathbf{g}^{RMC} + \Delta\mathbf{g}^{GC} \tag{2}$$

of which the "paramagnetic" second-order SO/orbital Zeeman cross term, $\Delta\mathbf{g}^{SO/OZ}$, dominates (except for extremely small $\Delta\mathbf{g}$ values).[34] Within our coupled−perturbed Kohn−Sham (CPKS) approach, using (nonlocally implemented) hybrid density functionals, and based on unrestricted Kohn−Sham calculations, its Cartesian components u and v are computed as

$$\Delta\mathbf{g}_{uv}^{SO/OZ} = \frac{\alpha^2}{2} g_e \left[\sum_k^{occ(\alpha)} \sum_a^{virt(\alpha)} \frac{\langle\psi_k^\alpha|\hat{\mathscr{H}}_v^{SO}|\psi_a^\alpha\rangle\langle\psi_a^\alpha|F'_{k,u}|\psi_k^\alpha\rangle}{\epsilon_k^\alpha - \epsilon_a^\alpha} - \sum_k^{occ(\beta)} \sum_a^{virt(\beta)} \frac{\langle\psi_k^\beta|\hat{\mathscr{H}}_v^{SO}|\psi_a^\beta\rangle\langle\psi_a^\beta|F'_{k,u}|\psi_k^\beta\rangle}{\epsilon_k^\beta - \epsilon_a^\beta} \right] \tag{3}$$

where α is the fine structure constant, $\hat{\mathscr{H}}_v^{SO}$ is explained below, and F'_K is the perturbed Fock operator, with $F'_K = l_O - (2/\alpha)a_0\sum_{k=1}^{n/2} K'_{k,v}$, where l_O is a spatial component of the orbital Zeeman operator, $K'_{k,v}$ is the response exchange operator, and a_0 is the weight of HF exchange, depending on the specific hybrid functional used. ψ^σ and ϵ^σ are spin-polarized Kohn−Sham orbitals and orbital energies, respectively. GGA or LDA functionals lead to an uncoupled DFT treatment for this second-order term ($a_0 = 0$). The relativistic mass correction term $\Delta\mathbf{g}^{RMC}$ and the one-electron part of the gauge correction term $\Delta\mathbf{g}^{GC}$ are also included in our approach[19] (see also refs 14 and 21 for related implementations).

Formalism of Hyperfine Tensor Calculations. The unrestricted Kohn−Sham calculations of most hyperfine structure data were done with the Gaussian98 program.[35] In these calculations, second-order corrections (due to SO coupling) to the hyperfine tensors are neglected. In this first-order approximation, isotropic hyperfine splittings $A_{iso}(N)$ correspond to the Fermi-contact term A^{FC}:

$$A_{iso}(N) = A^{FC} = \frac{4\pi}{3}\beta_e\beta_N g_e g_N \langle S_z\rangle^{-1} \sum_{\mu,\nu} P_{\mu,\nu}^{\alpha-\beta}\langle\phi_\mu|\delta(R_N)|\phi_\nu\rangle \tag{4}$$

Here, β_e is the Bohr magneton, β_N is the nuclear magneton, g_N is the g value of nucleus N, $\langle S_z\rangle$ is the expectation value of the z component of the total electronic spin, $P_{\mu,\nu}^{\alpha-\beta}$ is the spin density matrix, and the summation runs over all occupied molecular orbitals. The components T_{ij} of the anisotropic tensor are given by

$$T_{ij}(N) = \frac{1}{2}\beta_e\beta_N g_e g_N \langle S_z\rangle^{-1} \sum_{\mu,\nu} P_{\mu,\nu}^{a-\beta}\langle\phi_\mu|\mathbf{r}_N^{-5}(\mathbf{r}_N^2\delta_{ij} - 3\mathbf{r}_{N,i}\mathbf{r}_{N,j})|\phi_\nu\rangle \tag{5}$$

where $\mathbf{r}_N = \mathbf{r} - \mathbf{R}_N$ ($\mathbf{R}_N$ is the position vector of nucleus N). In the following, we will generally refer to the metal hyperfine interaction and the subscript N will be omitted.

SO corrections to **A** have been shown to give non-negligible contributions to the total **A** tensor.[15,16,18] Here, we calculated SO corrections to **A** with a recently developed approach.[36] The dominant SO correction term arises as a second-order coupling term. In this scheme, the SO contribution is written as a cross term between the one- and two-electron SO Hamiltonian $\hat{\mathscr{H}}^{SO}$ and the perturbed Fock operator F'_K:

$$\mathbf{A}_{K,uv}^{SO-I} = \frac{1}{2}\alpha^4 g_e \gamma_K \frac{1}{2\langle S_z\rangle} \left[\sum_k^{occ(\alpha)} \sum_a^{virt(\alpha)} \frac{\langle\psi_k^\alpha|\hat{\mathscr{H}}_u^{SO}|\psi_a^\alpha\rangle\langle\psi_a^\alpha|F'_{K,v}|\psi_k^\alpha\rangle}{\epsilon_k^\alpha - \epsilon_a^\alpha} - \sum_k^{occ(\beta)} \sum_a^{virt(\beta)} \frac{\langle\psi_k^\beta|\hat{\mathscr{H}}_u^{SO}|\psi_a^\beta\rangle\langle\psi_a^\beta|F'_{K,v}|\psi_k^\beta\rangle}{\epsilon_k^\beta - \epsilon_a^\beta} \right] \tag{6}$$

with $F'_K = l_v/r^3 - (2/\alpha)a_0\sum_{k=1}^{n/2} K'_{k,v}$, where l_v/r^3 is the paramagnetic nuclear-spin electron-orbit operator (detailed descriptions of our implementation are provided in ref 36; see ref 18 for a related CPKS implementation and both works for references to earlier implementations). For a better comparison with experimental values, the SO correction to **A** (*ii* denotes principal components) is given in terms of an isotropic pseudocontact (A^{PC}) and a traceless dipolar (T^{SOC}) term:

$$\mathbf{A}_{K,ii}^{total} = A_K^{PC} + T_{K,ii}^{SOC} \tag{7}$$

Computational Details. In the present work, the unrestricted Kohn−Sham orbitals have been obtained with the Gaussian98 program[35] and were transferred to the MAG-ReSpect property package[37] by suitable interface routines.[19] The following exchange-correlation functionals were compared: (a) the local density approximation in the form of the Vosko−Wilk−Nusair functional (VWN,[38] corresponding to the VWN5 keyword in the Gaussian98 code); (b) the BP86 GGA functional;[39,40] (c) the B3PW91 hybrid functional,[41−43] incorporating 20% HF exchange; and (d) user-defined one-parameter BPW91-based hybrid functionals (option of the Gaussian 98 program and, in the same way, taken for the MAG-ReSpect calculations) of the general form

$$aE_X^{HF} + (1-a)E_X^{B88} + E_C^{PW91} \quad (8)$$

with a (indicating the amount of HF exchange) chosen as 0.35, 0.5, and 0.6, in the following denoted as BPW91-35, BPW91-50 and BPW91-60.

The efficient and accurate atomic mean-field approximation[44,45] has been used to compute the matrix elements of the SO operator, $\mathscr{H}^{SO}$, in eqs 3 and 6. In the **g**-tensor calculations, we employed a common gauge at the transition-metal nucleus. The (15s11p6d)/[9s7p4d] metal basis set employed in our previous studies[20] has been used. DZVP basis sets[46] were used for the main group atoms without polarization *p* functions for hydrogen. The experimental structure of amavadin (crystallized with Ca^{2+} as a counterion; see ref 5) was used for calculations on the dianion. Structures optimized by Saladino and Larsen[27] were employed for $VO(gly)_2$ and $VO(H_2O)_5^{2+}$.

3. Results and Discussion

A number of experimental EPR spectra are available for comparison, both for amavadin itself[3,4] and for the smaller model complex $Ca[Ti(V)(hida)_2](H_2O)_6$.[2] These different spectra are similar but do not coincide. For example, the older spectra of amavadin[3,4] were analyzed as axial spectra, whereas the spectrum of McInnes et al. for the smaller model complex[2] exhibits moderate rhombicity. Moreover, both **g**- and **A**-tensor components exhibit a certain spread for the different experiments. This should be kept in mind in our comparisons of the calculations against the experimental values, which are shown for **g** tensors in Table 1 and for the ^{51}V **A** tensor in Table 2, as well as in Figures 2 and 3, respectively.

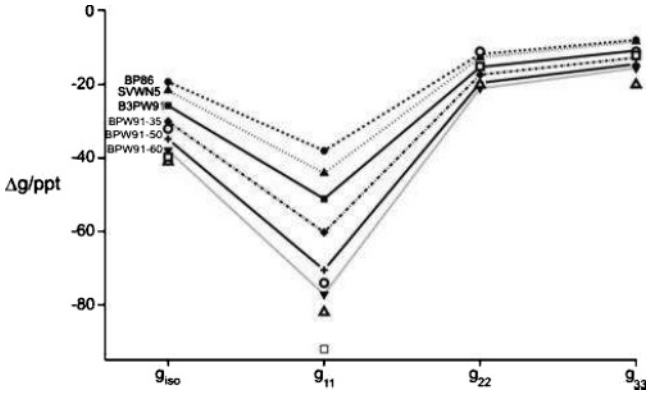

Figure 2. Dependence of computed **g**-shift tensors on the exchange-correlation functional. Open symbols indicate experimentally determined values.

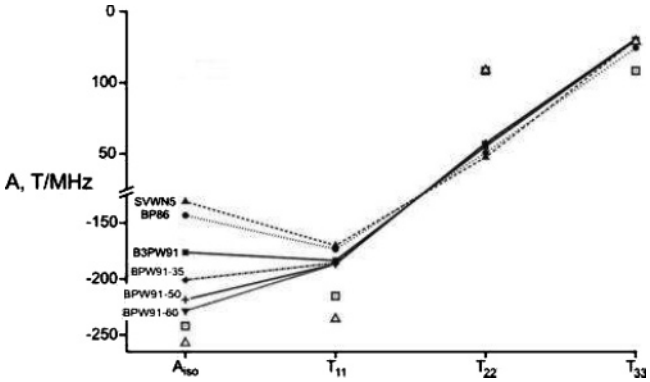

Figure 3. Dependence of computed **A** tensors on the exchange-correlation functional (isotropic and dipolar contributions). Open symbols indicate experimentally determined values.

TABLE 1: Comparison of Computed g-Shift Tensors for Amavadin (in ppt) with Experimental Values

method	Δg_{iso}	Δg_{11}	Δg_{22}	Δg_{33}	$\langle S^2\rangle^a$
SVWN5	−21.9	−44.4	−12.9	−8.5	0.758
BP86	−19.5	−38.3	−12.0	−8.1	0.758
B3PW91	−26.0	−51.4	−15.5	−11.0	0.766
BPW91-35	−30.3	−60.5	−17.6	−12.9	0.776
BPW91-50	−35.1	−70.8	−19.8	−14.7	0.790
BPW91-60	−38.2	−77.4	−21.3	−15.8	0.803
exp[b]	−41.3	−82.3	−20.3	−20.3	
exp[c]	−32.3(3)	−74.3(2)	−11.3(3)	−11.3(3)	
exp[d]	−40.0	−92.3	−15.3	−12.3	

[a] Expectation value for the Kohn−Sham determinant. [b] Frozen *A. muscaria* (cf ref 3). [c] *A. muscaria* in water (cf ref 4). [d] $Ca[Ti(V)(hida)_2](H_2O)_6$ (cf ref 2).

g Tensor. All of the functionals provide an appreciable **g**-tensor anisotropy, with all three **g**-shift components negative, as expected for a d^1 system. When going from the BP86 GGA functional to hybrid functionals with increasing the HF exchange admixture, the absolute value of the, by far, most negative **g**-shift component, Δg_{11}, increases and so does the **g**-tensor anisotropy [the local-spin-density-approximation (LSDA) functional SVWN-5 gives slightly better results than the BP86 GGA functional]. This improves the agreement with experimental values, at least up to an exact-exchange admixing coefficient a_0 of 0.5. With both 0.5 and 0.6, the computational results for Δg_{11}, and thus for Δg_{iso}, fall into the range of available experimental values. The dependence of Δg_{22} and Δg_{33} on the functional is, overall, somewhat less pronounced, and all of the results with hybrid functionals might be considered within the range of experimental data. Even for the hybrid functional with $a_0 = 0.6$, the spin contamination of the Kohn−Sham determinant remains moderate ($\langle S^2\rangle = 0.803$), and no appreciable problems for the **g** tensors are expected to arise from spin contamination for this early d^1 system (cf. Table 1). We note that the difference ($\Delta g_{22} - \Delta g_{33}$), that is, the asymmetry or rhombicity of the tensor, is computed to be about 4−5 ppt at all levels. This has to be contrasted with axial tensors for both experiments on amavadin itself[3,4] and with an asymmetry of ca. 3 ppt for $Ca[Ti(V)(hida)_2](H_2O)_6$.[2] We suspect that the experiments were not sufficiently accurate to resolve the asymmetry in the two former cases (cf. also below for the **A**-tensor results).

The A Tensor in the First-Order Approximation. Let us turn to the isotropic hyperfine coupling constant, A_{iso} (Table 2 and Figure 3). A similar dependence on the exchange-correlation functional as that observed for the **g** tensor is seen here. Increasing the HF exchange admixture moves the values closer to the range of experimental data (in contrast to the **g** tensors, BP86 is now closer to the experimental value than SVWN-5). However, even for $a_0 = 0.6$, the computational results are still 5−10% away from the experimental values (cf. Figure 3). As shown below, this discrepancy may be attributed to the neglect of second-order SO corrections in the calculations summarized in Table 2 and Figure 3. The dependence of the dipolar coupling contributions on the functional is much less pronounced than that for A_{iso}, as expected. The HF exchange admixture makes T_{11} somewhat more negative, but it remains ca. 15% above the range of experimental values at this nonrelativistic first-order level (see below). When averaged, the two perpendicular dipolar components T_{22} and T_{33} are also too small in absolute value relative to the (positive) experimental data. Moreover, the asymmetry ($T_{22} - T_{33}$) is much larger than that for the measured rhombic tensor of $Ca[Ti(V)(hida)_2](H_2O)_6$[2] (and the data from Gillard and Lancashire for amavadin were even fitted with an axially symmetrical tensor; cf. Table 2). A possible explanation

TABLE 2: Comparison of Computed Hyperfine Tensors for Amavadin (in MHz) with Experimental Values[a]

method	A_{iso}	T_{11}	T_{22}	T_{33}	A_{11}	A_{22}	A_{33}	$\langle S^2\rangle^b$
SVWN5	−131.6	−170.9	47.2	129.6	−302.5	−84.4	−2.0	0.758
BP86	−143.8	−174.3	50.3	124.0	−318.1	−93.5	−19.8	0.758
B3PW91	−177.0	−184.2	54.8	129.4	−361.2	−122.2	−47.6	0.766
BPW91-35	−201.6	−186.3	56.5	129.8	−387.9	−145.1	−71.8	0.776
BPW91-50	−219.2	−187.3	57.1	130.1	−406.5	−162.1	−89.1	0.790
BPW91-60	−229.3	−187.2	57.0	130.2	−416.5	−172.3	−99.1	0.803
exp[c]	−242.8	−215.9	107.9	107.9	(−)458.7	(−)134.9	(−)134.9	
exp[d]	(−)258.0	−236.4	108.1	128.3	(−)494.4	(−)149.9	(−)129.8	

[a] Nonrelativistic first-order results. [b] Expectation value for the Kohn−Sham determinant. [c] Frozen *A. muscaria* (ref 3). [d] $Ca[Ti(V)(hida)_2](H_2O)_6$ (ref 2).

TABLE 3: Influence of SO Corrections on Amavadin HFC Tensors (in MHz)

method	A^{FC}	A^{PC} (% of A^{FC})	A_{iso}^{total}	T_{ii}	T^{SOC} (% of T_{ii})	T_{ii}^{total}
				−174.3	−11.0 (6.3)	−185.3
BP86	−143.8	−12.4 (8.6)	−156.2	50.3	4.1 (8.1)	54.4
				124.0	6.9 (5.6)	130.9
				−184.2	−14.5 (7.9)	−198.7
B3PW91	−177.0	−15.5 (8.8)	−192.5	54.8	5.6 (10.2)	60.4
				129.4	9.0 (7.0)	138.4
				−187.2	−20.8 (11.1)	−208.0
BPW91-60	−229.2	−20.5 (8.9)	−249.7	57.1	8.3 (14.5)	65.4
				130.1	12.6 (9.7)	142.7

TABLE 4: Intermatrix Angles (deg) of Principal g and A Values of Amavadin

	A_{11}	A_{22}	A_{33}
	B3PW91 (Without SO Corrections for **A**)		
g_{11}	88.6	92.5	2.8
g_{22}	86.9	3.9	92.4
g_{33}	3.4	93.0	88.5
	B3PW91 (Including SO Corrections for **A**)		
g_{11}	90.2	90.1	0.2
g_{22}	89.9	0.2	90.1
g_{33}	0.2	90.1	90.2

could be that the calculations refer to a free dianion, whereas the experimental values should reflect influences of the counterion (hydrated Ca^{2+}) and of hydrogen bonds to surrounding water molecules. However, exploratory calculations with point charges or surrounding water and H bonds did not reduce the rhombicity of the computed tensor notably. We suspect that the experimental resolution was not sufficient to allow the rhombicity to be detected accurately.

Second-Order SO Corrections to the A Tensor. Table 3 provides second-order SO corrections to the **A** tensor (eq 6), given separately as contributions to A_{iso} and T. Both isotropic and dipolar parts of the **A** tensor are affected non-negligibly by the SO corrections, and in both cases, the computed values move closer to the range of experimental data. The SO contributions amount to ca. 6−14% of the nonrelativistic A_{iso} and T_{ii} values. Increasing the exact-exchange admixture increases the SO corrections, similarly to the **g** shifts (see above). In the second-order corrected framework, the hybrid functional with HF exchange coefficient $a_0 = 0.6$ now provides very close agreement with the experimental values for A_{iso} and T_{11} and, in part, for the average of T_{22} and T_{33}. However, the disagreement with the experimental values on the rhombicity of the tensor (see above) remains. In any case, the calculations show that, even for the early 3d metal vanadium, SO effects on metal hyperfine tensors may be non-negligible and should be included if one aims for accurate results.

Orientation of the Tensors. The orientations of the computed **g** and **A** tensors were evaluated with respect to the molecular framework and relative to each other (results were obtained with the MAG-ReSpect code). For both **A** and **g** tensors, the dominant "axial" component (A_{11} and Δg_{11}) points through the middle of the N−O bond of the two axial, side-on hydroxoimino ligands (Figure 4; this direction is generally denoted as the z axis). The

TABLE 5: Dependence of Mulliken Metal Spin Densities $\rho_{\alpha-\beta}$(V), Metal NPA Charges Q(V), and Metal Character of Singly Occupied NLMO on the Exchange-Correlation Functional

	$\rho_{\alpha-\beta}$(V)	Q(V)	V(SO-NLMO)
SVWN5	1.034	0.945	94.1%
BP86	1.085	1.044	96.1%
B3PW91	1.170	1.201	98.1%
BPW91-35	1.228	1.311	98.6%
BPW91-50	1.287	1.417	98.9%
BPW91-60	1.328	1.485	99.0%

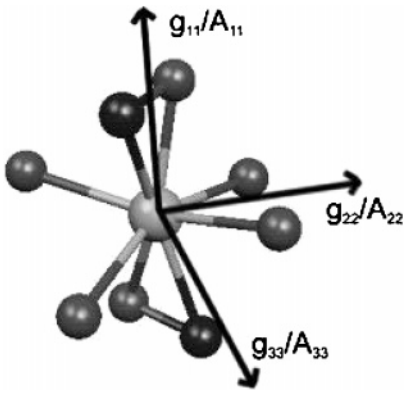

Figure 4. Computed orientation of **g** and **A** tensors in amavadin (B3PW91 result including SO corrections).

A_{22} and Δg_{22} components point along the bisecting line of the O−V−O angle of two adjacent carboxylato groups (Figure 4). Table 4 shows the deviation of the orientation of the two tensors relative to each other for two cases: (a) without and (b) with SO corrections to the **A** tensor. In the former case, small deviations ranging from 1.4° to 3.9° occur in the perpendicular (x, y) plane. After inclusion of SO corrections to the **A** tensor, both tensors are essentially coaxial. While the results in Table 4 were obtained with the B3PW91 functional, essentially the

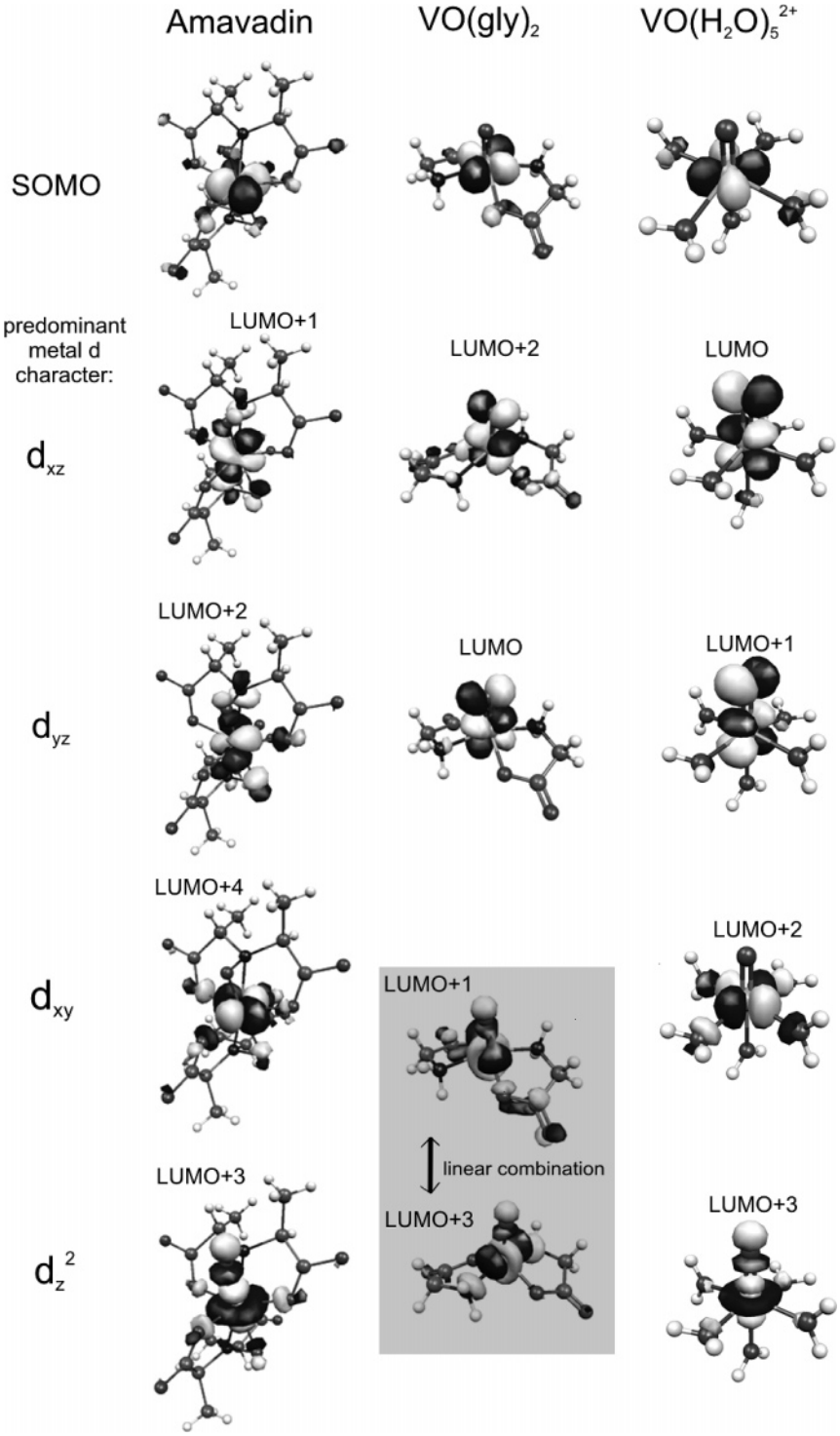

Figure 5. SOMO and virtual MOs relevant for $\Delta\mathbf{g}^{SO/OZ}$ and $\mathbf{A}^{SOC}$ in amavadin, $[VO(gly)_2]$, and $[VO(H_2O)_5]^{2+}$ (BP86 results). The dominant metal d character of the virtual MOs is indicated. Note that the virtual MOs are not ordered by energy but for consistency between the three complexes.

same conclusions are obtained with any of the exchange-correlation potentials studied here (BP86, B3PW91, and BPW91-60).

Understanding the Effect of the Exchange-Correlation Functional on Bonding and EPR Parameters. The largest ligand contributions to the SOMO arise generally from carboxylate oxygen p orbitals. The Mulliken spin population at vanadium ranges from ca. 1.0 for the BP86 GGA functional to ca. 1.5 for the hybrid functional with 60% HF exchange. The metal charge obtained from natural population analysis (NPA) increases from SVWN5 to BP86 to hybrid functionals. Simultaneously, the metal character of the singly occupied natural localized molecular orbital (NLMO), which was already 94% at the LSDA level, increases, in agreement with somewhat more ionic bonding (Table 5). This helps to rationalize the increased metal HFC with increasing the HF exchange admixture. Together with enhanced coupling terms (arising from the HF exchange contributions), similar arguments explain the increase in **g**-tensor anisotropy for hybrid functionals with increasing the HF exchange admixture.[19,47]

Similarity of the Amavadin EPR Parameters to Those of Vanadyl Complexes. As mentioned in the Introduction, it was the similarity of its EPR spectrum to spectra of vanadyl complexes that led to a long-standing misconception about the

TABLE 6: Comparison of Different Contributions to the g-Shift Tensor (BP86 Functional)[a]

amavadin				$VO(gly)_2$				$VO(H_2O)_5^{2+}$			
	Δg_{11}	Δg_{22}	Δg_{33}		Δg_{11}	Δg_{22}	Δg_{33}		Δg_{11}	Δg_{22}	Δg_{33}
Δg total	−38.3	−12.0	−8.1	**Δg** total	−29.7	−14.4	−9.5	**Δg** total	−43.1	−15.0	−14.4
$\Delta\mathbf{g}^{SO/OZ}$	−38.3	−11.9	−7.9	$\Delta\mathbf{g}^{SO/OZ}$	−29.7	−14.3	−9.3	$\Delta\mathbf{g}^{SO/OZ}$	−43.2	−14.8	−14.2
SOMO-LUMO+1 (d_{xz})[b]	0	0	−5.2	SOMO-LUMO+2 (d_{xz})[b]	0	−0.5	−6.5	SOMO-LUMO (d_{xz})[b]	0	0	−12.5
SOMO-LUMO+2 (d_{yz})[b]	−5.9	−9.6	0	SOMO-LUMO (d_{yz})[b]	0	−12.2	−0.5	SOMO-LUMO+1 (d_{yz})[b]	0	−13.3	0
SOMO-LUMO+4 (d_{xy})[b]	−33.1	−1.3	0	SOMO-LUMO+1 (d_{xy}/d_{z^2})[b]	−17.0	0	0	SOMO-LUMO+2 (d_{xy})[b]	−45.8	0	0
SOMO-LUMO+3 (d_{z^2})[b]	−1.1	−1.4	−1.3	SOMO-LUMO+3 (d_{xy}/d_{z^2})[b]	−14.7	0	0	SOMO-LUMO+3 (d_{z^2})[b]	0	0	0

[a] BP86 results. [b] Predominant metal d character for unoccupied MOs indicated. The numbering of virtual orbitals (LUMO+*x*) refers to the energy ordering of these orbitals.

structure of amavadin. Why are amavadin's EPR parameters so "vanadyl-like"? A vanadyl complex is typically composed of four equatorial ligands and one strongly bonded oxo ligand (usually expressed as a V═O double bond) in one of the axial positions. The other axial position either is occupied by a weakly bonded additional ligand or stays unallocated. As Armstrong et al. pointed out,[11] the ligand field in amavadin may indeed be strongest in the axial direction. While this is due to one strongly bound terminal oxo ligand in vanadyl complexes, the two η^2 NO^- ligands could create a similarly strong axial-ligand field. This was suggested by DV Xα calculations (that is, relatively approximate exchange-only local-density functional calculations) of orbital energies and the compositions of the orbitals.[11]

In Figure 5, we show the relevant orbitals (BP86 level) for amavadin and for two vanadyl complexes: $VO(gly)_2$, with only one ligand in the axial position, and $[VO(H_2O)_5]^{2+}$, with an additional weakly bonded axial water ligand trans to the oxo group. The SOMO is, in all three cases, essentially a metal $d_{x^2-y^2}$ orbital. In agreement with textbook knowledge on d^1 systems with $d_{x^2-y^2}$ SOMOs,[29,33] this explains, at once, the similarity of the HFC tensors for ^{51}V: the most negative **A**-tensor component has to point roughly in the axial *z* direction (the SO contributions are also largest in this direction; see below). The second-order $\Delta\mathbf{g}^{SO/OZ}$ term dominates the **Δg** tensor (eq 3). Analyses of $\Delta\mathbf{g}^{SO/OZ}$ in terms of contributions from specific orbital interactions have been compared for amavadin, $VO(gly)_2$, and $[VO(H_2O)_5]^{2+}$ (Table 6). The main contribution to the most negative Δg_{11} component (oriented in the *z* direction) arises from magnetic coupling of the SOMO with the lowest unoccupied molecular orbital (LUMO), which has essentially d_{xy} character [Figure 5; $VO(gly)_2$ does not exhibit a "pure" d_{xy}-type LUMO but rather two orbitals that are linear combinations with d_{xy} and d_{z^2} character). The same coupling dominates the largest component of the second-order corrections to the HFC tensor (eq 6). The less pronounced equatorial $\Delta\mathbf{g}^{SO/OZ}$ components arise mainly from couplings of the SOMO to unoccupied orbitals of d_{xz} and d_{yz} character (Figure 5 and Table 6). In all three cases, magnetic couplings between other orbitals are small (less than ±1 ppt) and are, therefore, not shown in Table 6.

4. Conclusions

Amavadin is a structurally fascinating vanadium complex whose biological role in mushrooms is still a matter of study. Here, the EPR parameters of amavadin have been analyzed in detail, and we used the complex to evaluate DFT methods for the computation of EPR parameters in transition-metal complexes. In particular, the influence of increasing amounts of HF exchange in hybrid functionals on both **g** and **A** tensors was evaluated. Even up to a 60% exact-exchange admixture, agreement with experimental values is still improved with nonlocal hybrid potentials. This is due to improved descriptions of metal−ligand bond ionicity (for both **g** and **A** tensors[47]) and enhanced metal core−shell spin polarization (for **A** tensors[20]). Because of the mainly nonbonding nature of the SOMO,[20] spin contamination of the Kohn−Sham determinant is not a problem for this early d^1 complex.

Second-order SO corrections account for ca. 6−10% of the computed isotropic and dipolar metal hyperfine tensor components and, thus, are clearly non-negligible in accurate calculations of this EPR parameter for amavadin (the same holds for the related vanadyl complexes). While the **g** and **A** tensors deviate very slightly from covariance when the **A** tensor is computed nonrelativistically, the second-order SO corrections make the two tensors almost coincide. Both tensors are strongly dominated by the axial direction given by the two η^2 NO^- ligands. This arises from the strong ligand field of these two groups and the resulting metal $d_{x^2-y^2}$ character of the SOMO. A similar character of the frontier orbitals in turn explains the close similarity of the EPR parameters of amavadin to those of vanadyl complexes, which has kept the structure of this interesting biological complex in the dark for such a long time.

Acknowledgment. This work has been supported by Deutsche Forschungsgemeinschaft (Schwerpunktprogramm "Hochfeld-EPR", SPP1051, Project KA1187/4) and by Fonds der Chemischen Industrie. C.R. also thanks "Studienstiftung des Deutschen Volkes" for a scholarship. Further support came from the graduate college "Moderne Methoden der Magnetischen Resonanz" at Universität Stuttgart. Support in Brno was provided via Grant LN 00A016 by the Ministry of Education of the Czech Republic. We are grateful to V. G. Malkin, R. Reviakine, and A. V. Arbuznikov for helpful comments.

References and Notes

(1) Bayer, E.; Kneifel, H. *Z. Naturforsch. B: Chem. Sci.* **1972**, *27*, 207.

(2) McInnes, E. J. L.; Mabbs, F. E.; Harben, S. M.; Smith, P. D.; Collison, D.; Garner, C.; Smith, G. M.; Riedi, P. C. *J. Chem. Soc., Faraday Trans.* **1998**, *94*, 3013−3018.

(3) Gillard, R. D.; Lancashire, R. J. *Phytochemistry* **1984**, *23*, 179−180.

(4) Krauss, P.; Bayer, E.; Kneifel, H. *Z. Naturforsch. B: Chem. Sci.* **1984**, *39B*, 829−832.
(5) Berry, R. E.; Armstrong, E. M.; Beddoes, R. L.; Collison, D.; Ertok, S. N.; Helliwell, M.; Garner, C. D. *Angew. Chem., Int. Ed.* **1999**, *38*, 795−797.
(6) Armstrong, E. M.; Beddoes, R. L.; Calviou, L. J.; Charnock, J. M.; Collison, D.; Ertok, N.; Naismith, J. H.; Garner, C. D. *J. Am. Chem. Soc.* **1993**, *115*, 807−808.
(7) Bayer, E.; Koch, E.; Anderegg, G. *Angew. Chem.* **1987**, *99*, 570−572.
(8) Carrondo, M.; Duarte, M. T.; Pessoa, J. C.; Silva, J. A. L.; Frausto da Silva, J. J. R.; Candida, M.; Vaz, T. A.; Vilas-Boas, L. F. *J. Chem. Soc., Chem. Commun.* **1988**, 1158−1159.
(9) Kneifel, H.; Bayer, E. *J. Am. Chem. Soc.* **1986**, *108*, 3075−3077.
(10) Garner, C. D.; Armstrong, E. M.; Berry, R. E.; Beddoes, R. L.; Collison, D.; Cooney, J. J. A.; Ertok, S. N.; Helliwell, M. *J. Inorg. Biochem.* **2000**, *80*, 6377.
(11) Armstrong, E. M.; Collison, D.; Deeth, R. J.; Garner, C. D. *J. Chem. Soc., Dalton Trans.* **1995**, 191−195.
(12) Kaupp, M.; Bühl, M.; Malkin, V. G. *Calculation of NMR and EPR Parameters: Theory and Applications*; Wiley-VCH: Weinheim, Germany, 2004.
(13) (a) Munzarová, M. L. Reference 12, pp 463−482. (b) Engels, B. Reference 12, pp 483−492. (c) Patchkovskii, S.; Schreckenbach, G. Reference 12, pp 505−532. (d) Lushington, G. Reference 12, pp 533−540.
(14) Schreckenbach, G.; Ziegler, T. *J. Phys. Chem. A* **1997**, *101*, 3388−3399.
(15) van Lenthe, E.; van der Avoird, A.; Wormer, P. E. S. *J. Chem. Phys.* **1998**, *108*, 4783−4796.
(16) Arratia-Perez, R.; Case, D. A. *J. Chem. Phys.* **1983**, *79*, 4939−4949.
(17) Patchkovskii, S.; Ziegler, T. *J. Am. Chem. Soc.* **2000**, *122*, 3506−3516.
(18) Neese, F. *J. Chem. Phys.* **2003**, *118*, 3939−3948.
(19) (a) Malkina, O. L.; Vaara, J.; Schimmelpfennig, B.; Munzarová, M; Malkin, V. G.; Kaupp, M. *J. Am. Chem. Soc.* **2000**, *122*, 9206. (b) Kaupp, M.; Reviakine, R.; Malkina, O. L.; Arbuznikov, A.; Schimmelpfennig, B.; Malkin, V. G. *J. Comput. Chem.* **2002**, *23*, 794−803.
(20) (a) Munzarová, M.; Kaupp, M. *J. Phys. Chem. A* **1999**, *103*, 9966−9983. (b) Munzarová, M. L.; Kubácek, P.; Kaupp, M. *J. Am. Chem. Soc.* **2000**, *122*, 11900−11913.
(21) Neese, F. *J. Chem. Phys.* **2001**, *115*, 11080−11096.
(22) Hieringer, W.; Della Sala, F.; Görling, A. *Chem. Phys. Lett.* **2004**, *383*, 115−121.
(23) Teale, A. M.; Tozer, D. J. *Chem. Phys. Lett.* **2004**, *383*, 109−114.
(24) Arbuznikov, A. V.; Kaupp, M. *Chem. Phys. Lett.* **2004**, *386*, 8−16.
(25) Arbuznikov, A. V.; Kaupp, M. *Chem. Phys. Lett.* **2004**, *391*, 16−21.
(26) Munzarová, M. L.; Kaupp, M. *J. Phys. Chem. B* **2001**, *105*, 12644−12652.
(27) Saladino, A. C.; Larsen, S. C. *J. Phys. Chem. A* **2003**, *107*, 1872−1878.
(28) Honzícek, J.; Nachtigall, P.; Císarová, I.; Vinklárek, J. *J. Organomet. Chem.* **2004**, *689*, 1180−1187.
(29) Abragam, A.; Bleaney, B. *Electron Paramagnetic Resonance of Transition Ions*; Clarendon Press: Oxford, U.K., 1970.
(30) Atherton, N. M. *Principles of Electron Spin Resonance*; Prentice Hall: New York, 1993.
(31) Weil, J. A.; Bolton, J. R.; Wertz, J. E. *Electron Paramagnetic Resonance: Elementary Theory and Practical Applications*; Wiley & Sons: New York, 1994.
(32) McGarvey, B. R. In *Transition Metal Chemistry: A Series of Advances*; Carlin, R. L., Ed.; New York, 1966; Vol. 3, pp 89−201.
(33) Mabbs, F. E.; Collison, D. *Electron Paramagnetic Resonance of d Transition Metal Compounds*; Elsevier: Amsterdam, 1992.
(34) Harriman, J. E. *Theoretical Foundations of Electron Spin Resonance*; Academic Press: New York, 1978.
(35) Frisch, M. J.; Trucks, G. W.; Schlegel, H. B.; Scuseria, G. E.; Robb, M. A.; Cheeseman, J. R.; Zakrzewski, V. G.; Montgomery, J. A., Jr.; Stratmann, R. E.; Burant, J. C.; Dapprich, S.; Millam, J. M.; Daniels, A. D.; Kudin, K. N.; Strain, M. C.; Farkas, O.; Tomasi, J.; Barone, V.; Cossi, M.; Cammi, R.; Mennucci, B.; Pomelli, C.; Adamo, C.; Clifford, S.; Ochterski, J.; Petersson, G. A.; Ayala, P. Y.; Cui, Q.; Morokuma, K.; Malick, D. K.; Rabuck, A. D.; Raghavachari, K.; Foresman, J. B.; Cioslowski, J.; Ortiz, J. V.; Stefanov, B. B.; Liu, G.; Liashenko, A.; Piskorz, P.; Komaromi, I.; Gomperts, R.; Martin, R. L.; Fox, D. J.; Keith, T.; Al-Laham, M. A.; Peng, C. Y.; Nanayakkara, A.; Gonzalez, C.; Challacombe, M.; Gill, P. M. W.; Johnson, B. G.; Chen, W.; Wong, M. W.; Andres, J. L.; Head-Gordon, M.; Replogle, E. S.; Pople, J. A. *Gaussian 98*, revision A.7; Gaussian, Inc.: Pittsburgh, PA, 1998.
(36) (a) Remenyi, C.; Reviakine, R.; Arbuznikov, A. V.; Vaara, J.; Kaupp, M. *J. Phys. Chem. A* **2004**, *108*, 5026−5033. (b) Arbuznikov, A.; Vaara, J.; Kaupp, M. *J. Chem. Phys.* **2004**, *120*, 2127−2139.
(37) Malkin, V. G.; Malkina, O. L.; Reviakine, R.; Arbouznikov, A. V.; Kaupp, M.; Schimmelpfennig, B.; Malkin, I.; Helgaker, T.; Ruud, K. *MAG-ReSpect*, version 1.1; 2003.
(38) Vosko, S. H.; Wilk, L.; Nusair, M. *Can. J. Chem.* **1980**, *58*, 1200.
(39) Perdew, J. P.; Wang, Y. *Phys. Rev. B: Condens. Matter Mater. Phys.* **1986**, *33*, 8822.
(40) Becke, A. D. *Phys. Rev. A: At., Mol., Opt. Phys.* **1988**, *38*, 3098.
(41) Becke, A. D. *J. Chem. Phys.* **1993**, *98*, 5648.
(42) Perdew, J. P. *Physica B* **1992**, *172*, 1.
(43) Perdew, J. P. In *Electronic Structure of Solids '91*; Ziesche, P., Eschring, H., Eds.; Akademie Verlag: Berlin, 1991.
(44) Hess, B. A.; Marian, C. M.; Wahlgren, U.; Gropen, O. *Chem. Phys. Lett.* **1996**, *251*, 365.
(45) Schimmelpfennig, B. *AMFI, Atomic Spin−Orbit Mean-Field Integral Program*; Stockholms Universitet: Stockholm, Sweden, 1996.
(46) Godbout, N.; Salahub, D. R.; Andzelm, J.; Wimmer, E. *Can. J. Chem.* **1992**, *70*, 560.
(47) Patchkovskii, S.; Ziegler, T. *J. Chem. Phys.* **1999**, *111*, 5730.